Trans. JWRI, Vol. 23 (1994), No. 1

Modeling and Characteristics of Through-the-arc Sensor†

Masao USHIO* and Wenjie MAO**

Abstract

Mathematic models of the through-the-arc sensor in GMA welding are developed, and compared precisely with an experiment. Through the modeling, the relationships between each loop hidden in the arc sensor system and the effects of the system parameters are made clear. Finally, an application of the sensor for the weld bead control is introduced.

KEY WORDS: (Arc Sensor) (Model) (Wire Melting) (Characteristics) (GMA Welding) (Weld Bead Control) (One-side Welding)

1. Introduction

A sensor is indispensable for automatic welding. In recent years, various types of sensors have been developed, and some have been used successfully in production processes. Among them, the through-the-arc sensor (simply called arc sensor) is most notice worthy because of advantages that include the possibility for real time control, no auxiliary parts around the torch, no need for maintenance and low cost[1].

In present paper, the modeling of the arc sensor is developed. Simulations on some phenomena of the arc sensor is made based on the models and discussed by comparison with experiments. Furthermore, an application of the sensor for the weld bead control in one side welding process with ceramic backing plate is introduced

2. Basic Principle of the Through-the-arc Sensor

In general, the output of the arc sensor is the welding current or the welding voltage, and the input is the torch height. Here, the torch height is defined as the sum of the wire extension and the arc length. The relationships between the output and the input are called as the characteristics of the arc sensor. If the input of the arc sensor is not changed with time, the relatinoship can be further called as static characteristic. Otherwise, the relatioships arc called as dynamic characteristic.

In gas metal arc welding (GMAW) processes, the welding current and voltage will vary while the torch height changes if the welding power source has a dropping characteristic of its output. For example, the welding current will change as shown in **Figure 1** because the torch height changes with the groove shape when the torch is oscillated across the groove by a specific mechanism. Therefore, the seam tracking can be realized by comparing of the wave forms or other characteristic values(Iml, Imr or Il, Ir) of the welding current in both sides of the center of torch weaving. If the welding current wave form shows symmetry, the torch center is just right on the seam line. Otherwise, the torch is miss aligned with the seam line.

The instance introduced above only used the dynamic characteristics of the arc sensor. In many applications, the static characterictic of the arc sensor is also useful, for example, in the control of the torch height[2].

† Received on July 11, 1994
* Professor
** Graduate student

Transactions of JWRI is published by Welding Research Institute of Osaka University, Ibaraki, Osaka 567, Japan.

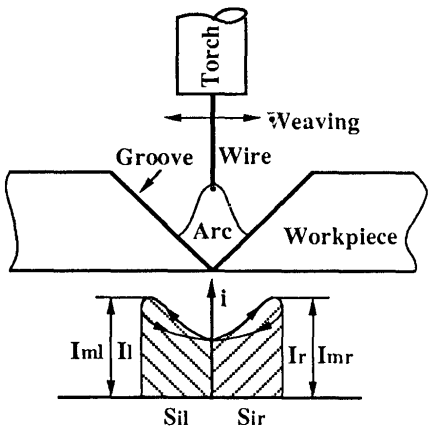

Fig.1 Principle of the through-the-arc sensor

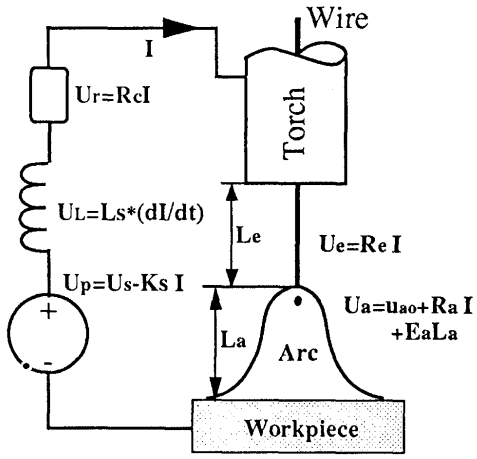

Fig.2 Equivalent electrical circuit of GMAW

3. Modeling of the Through-the-arc Sensor

Figure 2 shows the equivalent electrical circuit for GMAW processes. Where Ls, Ks, Rc and Re represent the inductance existed in the welding loop, the slope of output characteristics of power source, the resistance of cable and the resistance of wire extension respectively. The arc voltage drop is modeled with a constant component(uao) and components(Ra, Ea) proportional to welding current and arc length. The sum of all voltage drops in the loop should be equal to the electro-motive force(Us). Thus,

$$L_w\frac{dI}{dt}+(K_s+R_c+R_a+R_eI)=U_s-u_{ao}-E_a(L_t-L_e) \tag{1}$$

However, Le (wire extension) and Re are related to the wire melting behavior which is dominated by both the joule heat and the arc heat obtained at the tip of wire. So it is necessary to know the model of wire melting before solving Eq.1.

3.1 Model of wire melting

The temperature(T) distribution along the wire extension must satisfy the energy conversation equation (Eq.2) in which the heat loss due to radiation and that transferred to surroundings are neglected, and the heat conduction is only considered as one dimension.

$$\frac{1}{\partial Z}(\lambda(T)\frac{\partial T}{\partial Z})+\frac{I^2\rho(T)}{S^2(T)}=C_{ps}(T)\gamma(T)(V_f\frac{\partial T}{\partial Z}+\frac{\partial T}{\partial t}) \tag{2}$$

with the boundary conditions of

$$T(Z=0)=T_c$$

and $$T(Z=L_e)=T_m$$

Since the latter boundary moves with time t, further condition is necessary for determining the movement. Eq.3 takes account of the heat balance at the tip (included droplet) of wire. Namely, arc heat is balanced by the latent heat, the heat consumption due to the overheating of the droplet and the heat(Ha) transferred to extension by conduction. Where, the dLe/dt represents the moving rate of the tip of wire

$$H_a=\frac{I\phi}{(V_f-dL_e/dt)S_c\gamma_c}-(H_{latent}+C_{pl}\Delta T_d) \tag{3}$$

with the boundary conditions of

$$L_e(t=0)=L_{eo}$$

and $$T(Z,t=0)=T_o(Z)$$

Numerical calculations show that the effects of conduction in Eq.2 are less important to the temperature distribution along the wire extension, except near the wire tip of steel wires which have greater resistivity. This indicates that the joule heat generated at one place of wire extension would be almost used to raise its local temperature. Therefore, the following relationship will be obtained if the conduction term of Eq.2 can be omitted.

$$\int_{T_c}^{T}\frac{C_{ps}(T')S^2(T')\gamma(T')}{\rho(T')}dT'=\int_{t-Z/V_f}^{t}I^2(\tau)d\tau\equiv J_z \tag{4}$$

The left side is the function of variable temperature(T) only for a certain material and diameter of wire and the given Tc, while the right side is the joule heating weight Jz that takes into account the history of current experienced by an element which sets off the contact tip at the time Z/Vf (Vf constant) before t.

On the other hand, the heat content per unit mass of the same element can be calculated by

$$H_z=\int_{T_c}^{T}C_{ps}(T')dT' \tag{5}$$

The Hz expresses the joule heat content if the conduction effect is ignored. It is obvious that Hz is also the function of T only for the certain material and given

Tc. So Hz can be calculated by Jz. **Figure 3** shows the relationship between Hz and Jz obtained by experiments with steel wire (MIX-50S, dia. 1.2mm). The experiment method was similar to that proposed by Halmoy[3]. A constant current was applied to a segment of the wire in order to heat the segment uniformly. With the temperature increases, the voltage drop across the segment will change. The real time values were recorded by a digital recorder. Fig.3 shows that Hz changes almost linearly with Jz when Jz becomes greater. In fact, that interested in are the H_L and the J_L which represent the Hz and Jz at the tip of wire respectively. In usual welding conditions, J_L is greater and varies near the equilibrium point J_{Lo}, so the relationship can be fitted by a line shown as Fig.3. Considering the heat balance at the solid-liquid interface of the tip of wire, the sum of joule heat(H_L) and arc heat(H_a) should be equal to the heat content(H_m) of wire at the melting point. It yields the following equation which expresses the dynamic model of wire melting

$$\frac{dL_e}{dt} = V_f - \frac{A\,I}{1 - B\,J_L} \tag{6}$$

Where, $A = \phi / S_c \gamma_c \,(H_m + H_{latent} + C_{pl}\,\Delta T_d + a_0)$

and $B = a_1 /(H_m + H_{latent} + C_{pl}\,\Delta T_d + a_0)$

Because dL_e/dt is equal to zero in the steady state, the static model of wire melting can be derived from Eq.6 which is in agreement with that obtained by Halmay[3]. So the values of A and B can be determined through experiments of melting of wire in the steady state.

In order to verify the dynamic model of wire melting, we have measured the frequency response of wire melting to the supplied current which is changing as the sinusoidal wave form. **Figure 4** shows the results. A very good agreement between the nonlinear modeling and experiments is achieved.

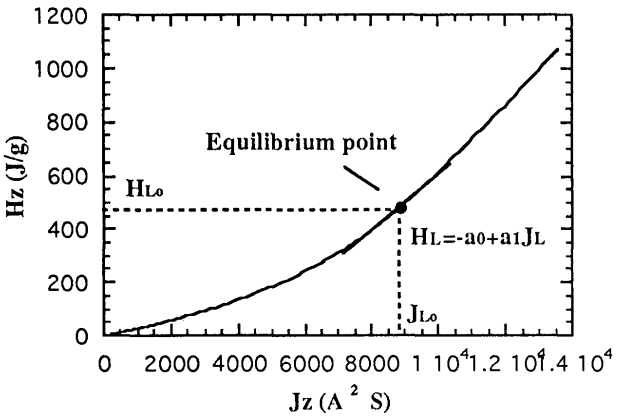

Fig.3 Relationship between the heat content(Hz) and the joule heating weight(Jz)

On the other hand, if welding parameters vary near the equilibrium point, the non-linear model can be approximated to linear. Namely, by deriving both side of Eq.6 with respect to time t, we can get the following equation .

$$\frac{d^2L_e}{dt^2} = -\frac{A}{1 - B\,J_{Lo}}\frac{dI}{dt} - \frac{A\,B\,I_o}{(1 - B\,J_{Lo})^2}\frac{dJ_L}{dt} \tag{7}$$

Because J_L is the function of variables the extension length and the welding current in the case of constant feeding rate of wire, the dJ_L/dt in Eq.7 can be expressed by

$$\frac{dJ_L}{dt} = \frac{\partial J_L}{\partial L_e}\frac{dL_e}{dt} + \frac{\partial J_L}{\partial I}\frac{dI}{dt} \tag{8}$$

Where, $\dfrac{\partial J_L}{\partial L_e} = \dfrac{\partial}{\partial L_e}\int_{t - Z/V_f}^{t} I_o^2\,d\tau = \dfrac{I_o^2}{V_f}$

and $\dfrac{\partial J_L}{\partial I} = \int_{t - Z/V_f}^{t} \dfrac{\partial}{\partial I} I(\tau)^2 d\tau = \dfrac{2 I_o L_{eo}}{V_f}$

which is derived from Eq.4. Substituting Eq.8 into Eq.7, the linear model of dynamic wire melting can be written as the following.

$$\frac{d^2L_e}{dt^2} + K_1\frac{dL_e}{dt} = -K_2\frac{dI}{dt} \tag{9}$$

Where, $K_1 = \dfrac{A\,B\,I_o^3}{(1 - B\,J_{Lo})^2 V_f}$

and $K_2 = \dfrac{A}{1 - B\,J_{Lo}} + \dfrac{2A\,B\,I_o^2 L_{eo}}{(1 - B\,J_{Lo})^2 V_f}$

3.2 Model of the arc sensor

The resistance of wire extension can be estimated by

$$R_e = \int_0^{L_e} r(J_z)\,dZ \tag{10}$$

It is known from the experiment with steel wires that the resistance r(Jz) per unit length of wire has two distinct range with J_z, and can be fitted approximately by following two curves. Where, J_{TP} corresponds to the

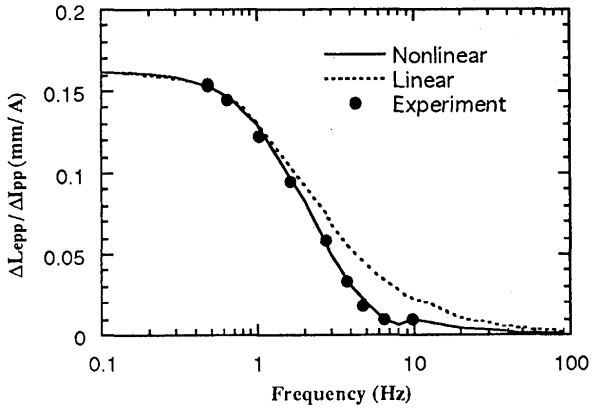

Fig.4 Frequency response of wire extension length to welding current

alpha to beta phase transfer temperature.

$$r = b_0 + b_1 J_z + b_2 J_z^2 \quad (J_z \le J_{TP})$$
$$r = c_0 + c_1 J_z \quad (J_z > J_{TP}) \qquad (11)$$

Thus the nonlinear model of the arc sensor can be obtained by combining of Eq.1, 6, 10 and 11. The corresponding linear model can also be derived from the nonlinear model based on the similar hypotheses mentioned above. The linear model of Re follows from

$$\frac{dR_e}{dt} = \frac{\partial R_e}{\partial L_e}\frac{dL_e}{dt} + \frac{\partial R_e}{\partial I}\frac{dI}{dt} \qquad (12)$$

Where, the partial difference terms can be derived from Eq.10 and 11. Because of $J_{Lo} \le J_{TP}$ in the present study,

$$\frac{\partial R_e}{\partial L_e} = \frac{\partial}{\partial L_e}\int_0^{L_e} r(J_z)dZ = r(J_{Lo}) \equiv r_o \quad \text{and}$$

$$\frac{\partial R_e}{\partial I} = \int_0^{L_{eo}} \frac{2I_o}{V_f}(b_1 Z + 2b_2 I_o^2 \frac{Z^2}{V_f})dZ \equiv \sigma$$

By derivation of Eq.1 with respect to time t and then substituting into Eq.12, it yields

$$L_w\frac{d^2I}{dt^2} + K_3\frac{dI}{dt} = -K_4\frac{dL_e}{dt} - E_a\frac{dL_t}{dt} \qquad (13)$$

Where, $K_3 = K_s + R_c + R_a + R_{eo} + I_o\sigma$

$K_4 = I_o r_o - E_a$

This way, the linear model can be obtained by combining of Eq.9 and 13.

4. Characteristics of the Arc Sensor

Based on the linear model of the arc sensor, its block diagram is drawn easily as **Figure 5**. By means of the block diagram, we can see clearly both the signal transfer directions and relationships at each loop in the arc sensor system. Here, the torch height change--- the input of the arc sensor may be caused by both the distance change between the torch and the workpiece and the weld pool surface position change. If there is a plus variation in the torch height, the welding voltage will immediately reponse to it and increase, but the welding curent will delay to responses to it because of the inductance included in the welding circuit. When the welding current decreased due to the welding voltage increase, the arc voltage inversely decrease for the plus feadback loop(R_a). On the other hand, the wire extension would extend for the minus feadback loop between the welding current and wire extension. So the arc length becomes shorter, and it finally result in the welding current and the welding voltage variation to become smaller. However, as you noticed from Fig.5, the wire extension response decays with the increase of the variation rate of the welding current. So the feaadback effects become less important when the variation frequency of the torch height is higher

On the other hand, simulations of the frequency responses of the arc sensor were made based on the models and the welding conditions and system parameters

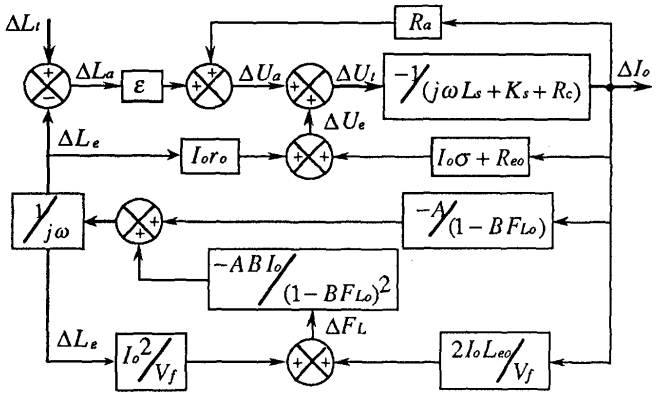

Fig.5 Block diggram of the through-arc arc sensor system

Table.1 Welding conditions and system parameters

$I_o = 280A$	$A = .23828\ mm/AS$
$V_f = 132.63mm/s$	$B = 5.5953\times10^{-5}A^{-2}S^{-1}$
$L_{eo} = 15mm$	$u_{ao} = 17.6V$
$\Delta L = 4.8mm$	$R_a = 0.02376\Omega$
$L_t = 21.5mm$	$E_a = 0.695V/mm$
$U_s = 34.3V$	$R_c = 0.0032\Omega$
$K_s = 0.01\Omega$	$\sigma = 4.64\ \mu\Omega/A$
$L_e = 600\mu H$	$r_o = .97m\Omega/mm$
$F_{Lo} = 8882A^2S$	

shown in **Table 1.** The results and experimental data are shown in **Figure 6** and **Figure 7** respectively. Good agreements are achieved between experiments and calculations, especially the results of nonlinear model.

It is seen that the sensitivity of the welding current is about constant in the range lower than 1Hz, but it increases rapidly above it and reaches the maximum at a frequency that is lower than 10Hz in usual welding conditions, and the frequency decreases with the inductance of the welding loop. Then, the sensitivity turns to decline The decrease rate increases with the inductance. The phase delay of the welding current relative to the torch height has the same change type as the sensitivity. It starts at 180 degrees and experiences both the decrease at first and the increase after it gets to the minimum. The phase delay is about 180 degrees when the gain reaches the maximum.

The sensitivity of the welding voltage increases monotonously with frequency. It becomes greater if there is greater inductance in the welding loop or a larger slope of output characteristics of the welding power source. In contrast with the welding current, the phase of the welding voltage advances than that of the torch height change. The phase lead is smaller at a very low(<0.3Hz) or quite high(>40Hz) frequency. Among the medium frequency range, especially from 1Hz to 10Hz, the phase lead is greater but less than 90 degrees in general. The

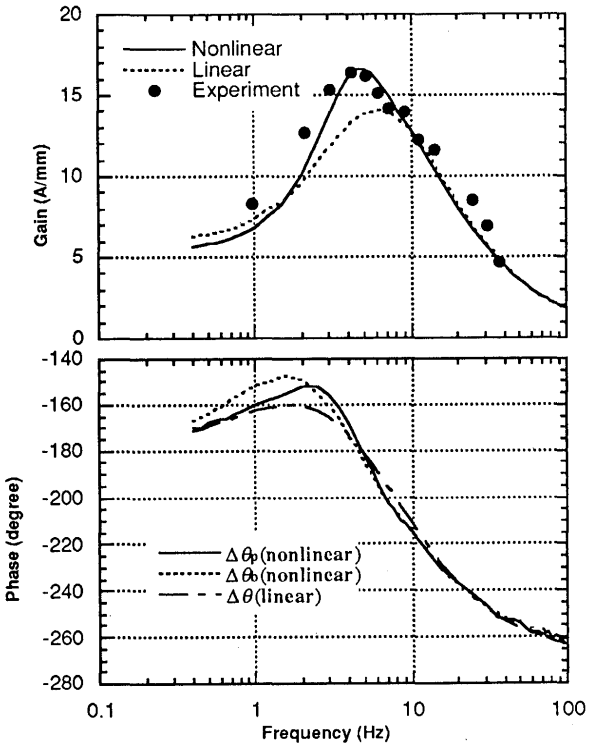

Fig.6 Frequency response of welding current to torch height change

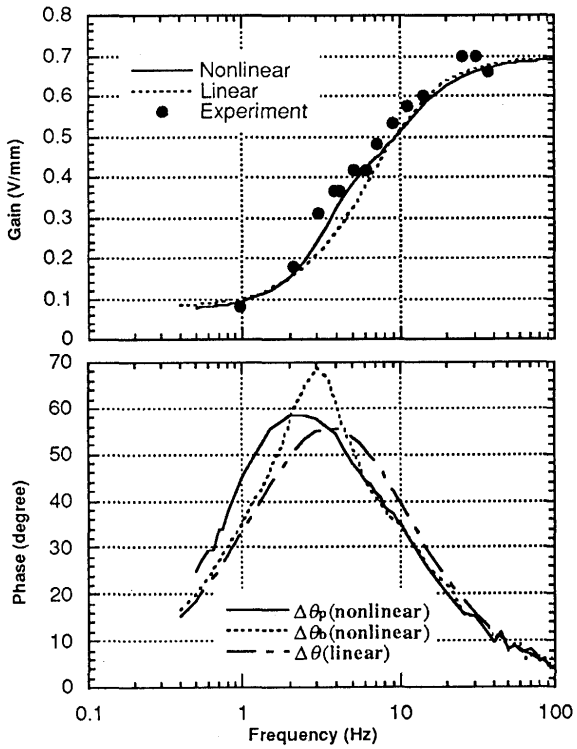

Fig.7 Frequency response of welding voltage to torch height change

other parameters also affect the characteristics of the arc sensor. In relatively low or high frequency range, you can simply learn some effects by following equations derived from the linear model(Lw=0H)

$$\frac{\Delta I}{\Delta L_t} = \frac{K_1}{K_1K_3 - K_2k_4} \quad \text{(in low frequency range)}$$

$$\frac{\Delta I}{\Delta L_t} = \frac{E_a}{K_3} \quad \text{(in high frequency range)} \tag{14}$$

5. An Application of the Arc Sensor for the Adaptive Control of Weld Bead Shape

A consistent weld bead shape is usually expected in a one-side welding process. Unfortunately, it is often imperiled by the groove geometry variations which are difficult to avoid due to the thermal distortions and the assembled errors of the workpiece. In order to overcome these disturbances, a new welding parameters control strategy has been developed that uses a high welding current and the high speed rotating arc welding process. In this method, only the wire feeding rate and welding power source output characteristics are regulated according to the groove shape. The other parameters like the welding current, arc length and arc voltage, as well as welding speed, are all not subjected to change. Experimental results have proved that the method is effective for achieving a consistent weld bead regardless

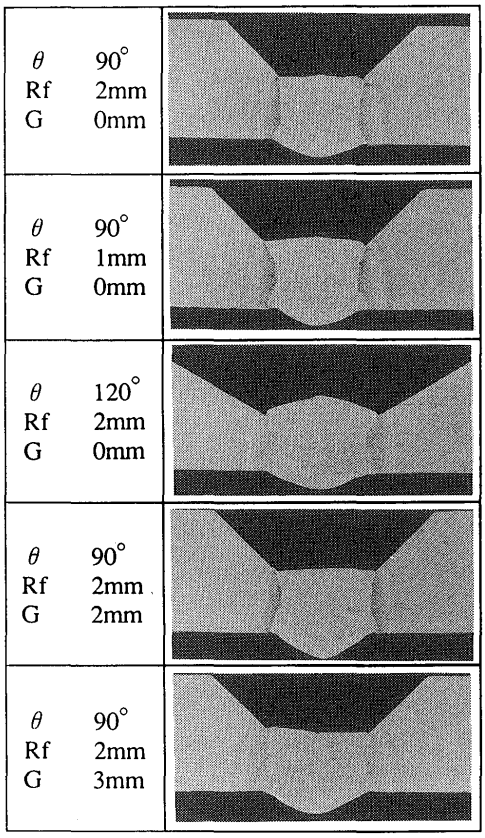

Fig.8 Results of weld bead shape control with arc sensing technique

of groove shape changes. Now the problem is how to learn the information on the variations of groove shape. It is found that the arc length exactly in the rear of the rotating cycle of arc becomes longer or shorter while the cross-section area of the groove becomes larger or smaller. This information can be detected without difficulty using the welding voltage or current in the case of dropping output characteristics of welding power source.

Thus, an automatic welding system for the control of weld bead has been developed. In the system, the seam tracking, the torch height control and the control of weld bead are all completed by the arc sensing technique. The preliminary experimental results made by the system are shown in **Figure 8**. It is seen that the satisfactory weld bead shapes are achieved regardless of how the geometry of groove varies.

6. Conclusion

The modeling of the arc sensor in GMAW helps us have a good insight into its behavior in a dynamic state. The models of wire melting and arc sensor have been developed and verified by experiments. The main points included in the paper are the following:

(1) GMAW acts as a low pass filter for wire melting responding to the welding current. If the variation frequency of the welding current exceeds 10Hz, the wire extension shows little response.

(2) The block diagram for arc sensor system(Fig.5) provides insight into the relationships between each loop hidden in the arc sensor system.

(3) The wire melting behaviours and the inductance of the welding loop dominate the main dynamic behaviors of the arc sensor. The highest sensitivity of the welding current appears at a frequency which is lower than 10Hz in usual welding conditions and decreases with the inductance. However, the sensitivity of the welding voltage increases monotonously with frequency and the inductance. Other system parameters such as the slope of the output characteristics of the power source or the resistance of the welding loop will make the sensitivity of the welding current smaller but increase the sensitivity of the welding voltage.

(4) The phase of the welding current delays to that of the torch height. The phase delay is about 180° at the frequency corresponding to the maximum response of the welding current. In contrast, the phase of the welding voltage advances to that of torch height. The phase lead is only little in the very low or quite high frequency range.

(5) Utilizing the arc sensor, not only can the seam tracking and torch height control be realized, the adaptive control for a weld bead can also be completed. With further work to better understand the interactions between the arc, the welding position and the weld pool, the application of the arc sensor is sure to widely expand

Acknowledgement

The authors would like to thank very much Dr.Yuji Sugitani of Engneering Reseach Center of NKK for the offering of a part of the experimental materials and very useful advises

Simbols

A, B:	Coefficients of wire melting model
a_0, a_1:	Coefficients in fit of joule heating content of electrode wire $H_L(J_L)$
b_0,b_1,b_2:	Coefficients in fit of electric resistance per unit length of the wire extension
c_0,c_1:	Coefficients in fit of electric resistance per unit length of the wire extension
C_{pl}:	Specific heat of wire in liquid state (J/g K)
$C_{ps}(T)$:	Specific heat of wire in solid state (J/g K)
E_a:	Electric field intensity in arc column (V/mm)
J_L:	Joule heating weight at the wire tip (A^2 S)
J_{Lo}:	Joule heating weight at the wire tip and in equilibrium state(A^2 S)
J_Z:	Joule heating weight of wire extension at the distance Z away from contact tip
H_a:	Arc heating content at the wire tip (J/g)
H_{JL}:	Joule heating content at the wire tip (J/g)
H_{Jz}:	Joule heating content of wire extension at the distance Z away from contact tip (J/g)
H_{latent}:	Latent heat of electrode wire (J/g)
H_m:	Heat content of electrode wire at melting point (J/g)
I:	Welding current (A)
I_o:	Welding current in equilibrium state (A)
K_s:	Slope at the equilibrium point of the static characteristic of power source (V/I)
L_a:	Arc length (mm)
L_e:	Wire extension length (mm)
L_{eo}:	Wire extension length in equilibrium state (mm)
L_t:	Torch height (mm)
L_w:	Inductance of welding loop (H)
R_a:	Electric resistance of arc column (ohm)
R_c:	Resistance of cable (ohm)
R_e:	Total resistance of wire extension (ohm)

R_{eo}: Total resistance of wire extension in equilibrium state (ohm)
$r(f_z)$: Resistance of wire extension per unit lenght (ohm/mm)
r_o: Resistance of wire extension per unit lenght at the equilibrium point (ohm/mm)
S(T): Cross-sectional area of wire (mm^2)
S_c: Cross sectional area of wire at the contact tip (mm^2)
T: Temperature of wire (K)
T_c: Temperature of wire at the contact tip (K)
T_m: Temperature of wire at melting point (K)
$T_o(Z)$: Temperature at the distance Z away from contact tip and in equilibrium state (K)
ΔT_d Overheat temperature of droplet
U_a: Arc voltage (V)
u_{ao}: Constant component of arc voltage (V)
U_e: Voltage drop across wire extension (V)
U_p: Output voltage at the terminals of welding power source (V)
U_s: Equivalent output voltage of welding power source in the state of I=0 (Equivalent electro-motive force)
U_t: Welding voltage ($=U_a+U_e$) (V)
V_f: Wire feeding rate (mm/s)
Z: Distance along the wire extension away from contact tip (mm)
ϕ: Equivalent wire melting voltage of arc (V)
$\lambda(T)$: Conductivity of wire (J/mm S K)
$\gamma(T)$: Density of wire (g/mm^3)
γ_c: Density at the contact tip of wire
$\rho(T)$: Resistivity of wire (ohm mm)
σ: Value of $\frac{\partial R_e}{\partial I}$ in equilibrium state

Reference

1) Welding Guide Book 2: "Sensors and Control Systems in Arc Welding," Technical Commission on Welding Process, Japan Welding Society;
2) H. Nomura, Y. Sugitani and M. Murayama: "Development of Automatic Fillet Welding Process with High Speed Rotating Arc," IIW XII-939-86 (1986);
3) E.Halmoy: "Wire Melting Rate, Droplet Temperature and Effective Anode Melting Potential," The Int'l Conference on Arc Physics and Weld Pool Behavior, in London, 8-10 May 1979.